A Magnetic Continuum Device with Variable Stiffness for Minimally Invasive Surgery

Christophe Chautems, Alice Tonazzini, Quentin Boehler, Seung Hee Jeong, Dario Floreano, Bradley J. Nelson*

Dr. C. Chautems,
Multi-Scale Robotics Lab, Tannenstrasse 3, ETH Zurich, 8092 Zurich, Switzerland
E-mail: chautemc@ethz.ch

Dr. A. Tonazzini
Laboratory of Intelligent Systems, EPF Lausanne, 1015 Lausanne, Switzerland

Dr. Q. Boehler
Multi-Scale Robotics Lab, ETH Zurich, 8092 Zurich, Switzerland

Dr. S. H. Jeong,
Laboratory of Intelligent Systems, EPF Lausanne, 1015 Lausanne, Switzerland

Prof. D. Floreano,
Laboratory of Intelligent Systems, EPF Lausanne, 1015 Lausanne, Switzerland

Prof. B. J. Nelson,
Multi-Scale Robotics Lab, Tannenstrasse 3, ETH Zurich, 8092 Zurich, Switzerland
E-Mail: bnelson@ethz.ch

Keywords: soft robotics, variable stiffness system, continuum robot, magnetic navigation, medical robotics

One of the challenges of minimally invasive surgery is the dexterous manipulation and precise control of small diameter continuum surgical instruments. In this paper, a magnetic continuum device with variable stiffness (VS) is presented, whose tip can be precisely shaped and controlled using an external magnetic field. Based on a low melting point alloy (LMPA), the serial segments composing the continuum device can be independently softened via electrical current and remotely deformed under a magnetic torque while the rest of the device is locked in place. The resulting system has the advantage of combining the precision of magnetic navigation with additional degrees of freedom provided by changing the segments stiffness. With a minimum diameter as small as 2.33 mm and an inner working channel, the magnetic continuum device with variable stiffness can be adapted for use in several

therapeutic scenarios, including radio frequency cardiac ablations and interventional endoscopy in the gastrointestinal tract. The magnetic torque is used to remotely control the shape of the soft sections while the stiff sections remain unchanged, thus adding degrees of freedom to the magnetic continuum device.

1. Introduction

Minimally invasive instruments are inserted in the human body through small incisions or natural lumens, leading to less trauma and shorter patient recovery time compared to conventional surgical approaches. Among these instruments, flexible continuum devices can safely access difficult-to-reach areas via tortuous pathways, thus enabling new minimally invasive surgical scenarios as well as enhancing existing therapies. Since the anatomy of body cavities is often complex and patient-specific, dexterity and controllability in a confined space are important features for such flexible continuum devices to be successfully used in fields such as neurosurgery and abdominal or cardiac surgery.[1]

In order to navigate through the workspace, tendon/cable actuation is commonly used for deflecting the tip of continuum devices.[2] For example, in most manual catheters used for radiofrequency (RF) ablation of cardiac arrhythmias, the tip position is controlled by rotating/pushing/pulling the catheter shaft into its sheath and by deflecting the tip with pull wires attached to the distal end of the flexible catheter. Cables, together with other extrinsic actuation mechanisms such as multi-backbone structures[3] and concentric tubes[4], suffer from high friction (e.g. passing tension wires through complex paths) and are limited in their ability to provide multiple bends in a small diameter. Alternative actuation systems include fluidic actuation[5] (usually proposed for larger diameter devices), shape memory alloys [6,7] (raising the issue of precise control), and magnetic actuation [8][9][10]. In magnetic actuation, an external

magnetic field is used to control the pose of the magnetic tip of a continuum device.[8] This remote magnetic navigation approach allows for contactless actuation without the need for transmissions systems running along the device shaft. Unfortunately, even if multiple magnets can be integrated into a single tool, different magnetic field directions cannot be applied at different magnet positions in the workspace inside our magnetic navigation system. Therefore, it is not currently possible to navigate through the body by adopting multiple curvatures in 2D and 3D without using support provided by contact with body cavities (e.g. heart walls in the case of cardiac ablation procedures).

Commercially available magnetic catheters are primarily used for treating cardiac arrhythmias [8] while other proposed applications (e.g. brain [11], lung [12], cochlear [13], and eye [14] surgeries) are still far from clinical practice. Such catheters are composed of an ablation tip, flexible segments, and permanent magnets.[15] The number of permanent magnets and the distance between them (i.e. the length of the interposed flexible segment) are optimized for achieving a suitable alignment of the tip to the applied external magnetic field.[18]

To provide stability during operation, the integration of variable stiffness (VS) backbones and outer tubes into non-magnetically guided instruments is a well-known solution, particularly for instruments operating in the intestine and in the abdomen.[16] A number of different designs have been proposed based on tension-stiffening of friction-locking beads [17], combinations of concentric tubes [18], phase change materials [19], and granular and layer jamming.[20] [21] Among intravascular continuum devices, given the dimension constraints, few examples can be found based on material stiffening (i.e. using materials that undergo stiffness variation under certain stimuli), and are mainly limited to low melting point materials (e.g. polymers [22] and alloys [23]).

In our previous paper, we demonstrate the advantages provided by the combination of remote magnetic navigation and variable stiffness for minimally invasive continuum devices.[24] Selectively locking one or more flexible segments of a continuum device enables instruments

capable of several degrees-of-freedom despite the application of a single magnetic field. Therefore, complex 2D and 3D shapes can be achieved and a wider workspace can be reached. Moreover, the entire structure can be stiffened during a surgical procedure to improve tool stability. The stiffness change is based on a low melting point alloy (LMPA), where serial segments independently undergo a significant stiffness variation (solid to liquid and vice-versa) within a bio-compatible temperature range (melting temperature below 50°C).

In this paper, we introduce a new design with a central working channel and feedback for closed-loop temperature control **(Figure 1)**. The working channel can be used to connect a functional tip or to insert a tool for applications such as cardiac ablation and gastro-intestinal surgery. The closed-loop temperature control averts an overheating and potential damage to the cells. The addition of those two features is achieved without increasing the external diameter of 2.33mm and overcome two major limitations of our previous design.

2. Materials and Methods

2.1. Variable stiffness continuum devices

We designed and developed different VS continuum devices based on the structure, dimensions, and requirements of existing magnetic catheters.

For efficient shaping, the VS catheter segments should easily bend in the soft state and align in the direction of the magnetic field. For under-actuation and stability during end effector operation, in the stiff state the VS catheter segments should resist the bending torque due to magnetic field (i.e. 2 x 10^{-3} Nm) and the contact force between the VS catheter tip and human tissues (e.g. 0.2 N between heart wall and catheter tip during the ablation [25]). The diameter of the VS catheter should be approximately 2.33 mm, which is the current standard for cardiac catheters. [26]

Given the spatial constraints and the mechanical features needed inside the magnetic field, we chose low melting point alloys (LMPAs) as a variable stiffness strategy. LMPAs are alloys

whose solid/liquid phase change occurs at relatively low temperatures. [27] They are characterized by a large stiffness change upon phase change and by high absolute stiffness when solid.[28] Their potential use in biomedical applications (e.g. micro devices for vessel exploration, material for bone repair) is of current research interest.[29] Among LMPAs, Cerrolow 117 (composition by weight: 45% bismuth, 23% lead, 19% indium, 8% tin, 5% cadmium) has a 47°C melting temperature and is stable in air. Below the melting temperature, it is a solid characterized by a Young modulus of 3 GPa, a tensile strength of tens of MPa, and strain-at-break of around 3% (mechanical characterization described in [28]). Above the melting temperature, the material is a liquid with low viscosity. Cerrolow 117 undergoes phase change faster than other phase change materials (i.e. wax and SMP) due to its much higher thermal conductivity.[30,31] As the material is liquid at higher temperatures and contains toxic elements such as cadium and lead, Cerrolow 117 requires encapsulation.

Figure 2 shows the VS continuum device with a central working channel that can be used for active cooling (e.g. irrigation fluid passes through the inner pipe, **Figure S1-A**) or for cable actuation (e.g. a cable running through the inner channel for actuating a gripper, **Figure S1-B**) depending on the surgical scenario. Fabricated according to **Figure S2** (see Fabrication in supplementary text for details), the prototype is composed of an inner flexible tube, Cerrolow 117, three heaters, a magnet and a silicone tube that encapsulates the entire structure. The external diameter is 2.5 mm. The three heaters consist of enameled copper wire coiled around the inner tube, corresponding to three independent variable stiffness segments (VSSs) (see Fabrication in supplementary text for details). The flexible inner tube is coaxial to the tubular structure of the continuum device and separated by plastic spacers. The spacers are equally spaced on the circumference (120° from each other) and along the length of the flexible tube (15 mm), where they delimit the VS segments (**Figure 2**, section B-B). The space between the flexible inner tube and the outer silicone tube is occupied by LMPA. This LMPA distribution allows for an increased moment of inertia of the continuum device cross section compared to

a backbone-like distribution with the same cross-sectional area, which maximizes its bending stiffness in the stiff state. Silicone encapsulation is important not only for containing the molten alloy but also for thermal insulation (thermal conductivity at 100°C is in the range of 0.2-0.3 $Wm^{-1}K^{-1}$), electrical insulation, and biocompatibility with human tissues and body fluids.

When current (e.g. 0.8-1 A) is injected into the heaters, the temperature of the LMPA increases above the melting temperature and the VSS becomes soft. In this state, the mechanical performance of the VSS is roughly that of the outer silicone tube. [28,30] Within an external magnetic field, the soft VSS behaves like the flexible segments in standard continuum devices, allowing the alignment of the magnet with the direction of the magnetic field. When the LMPA solidifies inside the magnetic field, the VSS becomes rigid and retains the deformed shape. In this state, the LMPA core sustains tensile and compressive loads (e.g. due to the magnetic field oriented in a different direction compared to the magnet direction), while the contribution to device stiffness from silicone encapsulation is negligible.

A reheating-and-cooling cycle applied to the deformed and/or fractured VSS restores its original straight shape (i.e. the shape of the unloaded silicone encapsulation) and its mechanical properties in the solid state (i.e. Young modulus, maximum stress and strain). Such a restoration of the mechanical properties after fracture (i.e. self-healing) also occurs in the presence of an external magnetic field[30]. Restoration is due to the pre-stretched state of the silicone encapsulation obtained during fabrication (see **Figure S2** steps D-E and Fabrication).

The LMPA is radiopaque and, thus, is visible in X-Ray images (Movie S3). During an ablation procedure this feature allows the electrophysiologist to monitor the position of the catheter with a mapping system and a fluoroscope.

Each heater, which is implemented by enameled copper wire wrapped around either the flexible inner tube or directly on the LMPA, is a closed electric circuit. One end of the copper

wire runs along the encapsulated structure to the base (i.e. toward the external part of the device, see Fabrication). One part of the copper wire constitutes the heater itself, being tightly wrapped around the section to be heated. The second end of the copper wire is connected to ground either externally (i.e. by running along the structure to the base like the other end) or through the LMPA (see Fabrication).

2.2. Stiffness control

As previously mentioned, the stiffness of each VSS depends on the phase of the LMPA, which can be locally and independently changed by Joule heating. The enameled copper wires wrapped around the core of the catheter (see 2.1 and Fabrication) define separate VS segments and serve as both heaters (where current is injected to melt the LMPA) and temperature sensors. This minimizes the number of electric wires running along the structure, decreasing device complexity and increasing space for other components. The temperature of the heater T_h is related to the the copper wire resistance R_h as:

$$R_h = R_0(1 + \alpha(T_h - T_0))$$

where the temperature coefficient α of the copper is equal to 3.9 x 10^{-3} °C^{-1}, and R_0 is the wire resistance at an initial temperature T_0.

In a surgical scenario, the temperature varies between 37°C (body temperature) and 47°C (melting temperature of the LMPA). This implies that very low resistance variations must be monitored. Resistance measurement is performed with a high precision resistance measurement terminal (EL3692, Beckhoff Automation AG, Germany) connected to the heater with a 4-wire connection in parallel with a power supply. The components of the setup are coupled to an EtherCAT fieldbus, and the overall setup is controlled with a TwinCAT PLC Control running a real-time operating system. Heating is performed by applying a PWM voltage signal across the heater. The resistance measurement is performed on each low state of the PWM signal so that both heating and resistance measurements are performed

alternatively using the same wires. The current used for the resistance measurement is lower than 45 mA, and its influence on the wire heating is negligible with respect to the heating current produced by the power supply (i.e. 0.8-1 A).

A VSS can be maintained in the soft state by injecting current so that the heater resistance remains between a lower and upper bound using a hysteresis controller. The lower bound is set slightly above the resistance corresponding to the LMPA melting temperature. The upper bound is set close to the lower bound to avoid overheating the LMPA. Both resistance thresholds are experimentally identified with an initial testing of the device (see section 3.1).

2.3 Actuation and modeling

2.3.1 Magnetic actuation

Remote magnetic navigation is performed with a Magnetic Navigation System (MNS). Such systems usually use either static electromagnets or moving permanent magnets to generate a magnetic field within a given volume. [32] The permanent magnet embedded at the distal end of the flexible continuum device is subjected to a magnetic torque that attempts to align it with the external field direction, allowing control of the device tip position with the MNS. In an external magnetic field $\boldsymbol{B}$, the magnet in the continuum device tip, characterized by a magnetic dipole m and a position $\boldsymbol{p}$, experiences a magnetic torque

$$\boldsymbol{T}_m(\boldsymbol{m},\boldsymbol{p}) = \boldsymbol{m} \times \boldsymbol{B}(\boldsymbol{p}). \quad (1)$$

This torque is proportional to the magnetic field magnitude. It is equal to zero when the magnetic dipole m is aligned with the magnetic field $\boldsymbol{B}$, and is maximal when $\boldsymbol{B}$ and m are orthogonal if the magnetic material on the catheter is permanently magnetized.[33]

2.3.2 Device modeling

The magnetic continuum device is modeled with an Euler-Bernoulli beam model assuming a constant curvature along the length of the device, as previously proposed in [34]. Using the same assumption as Tunay for a thin body [35], we assume that the plane sections of the

continuum device remain in-plane and perpendicular to the neutral-fiber axis after deformation, and the shear deformation is negligible. In this case, we have

$$\kappa = \frac{\boldsymbol{T_m}}{\boldsymbol{EI}} \tag{2}$$

where T_m is the bending moment, $\boldsymbol{E}$ is the Young modulus of the elastic material, $\boldsymbol{I}$ is the area moment of inertia, and κ the segment constant curvature.

Equation (1) can be rewritten using the magnetic field norm $\boldsymbol{B}$ and the dipole moment norm $\boldsymbol{m}$ to obtain the magnetic torque norm

$$\boldsymbol{T_m} = \boldsymbol{Bm}\sin(\gamma - \theta) \tag{3}$$

where γ denotes the magnetic field inclination angle, and θ is the inclination angle of the tip magnet. From equation (3) we can observe that a misalignment angle $\gamma - \theta$ between the external magnetic field and magnet direction is required to apply a control torque on the magnet. No magnetic torque can be generated around the dipole axis. For the considered device and magnetic field intensity, the influence of gravity on the device position is negligible. The influence of the force produced by the magnetic gradients is also negligible, as the magnetic field produced by the MNS is essentially homogeneous.

Using the conversion between magnet inclination angle and curvature $\theta = \kappa \boldsymbol{l}$ and, combining equations (2) and (3), we obtain:

$$\theta = \frac{\boldsymbol{lBM}}{\boldsymbol{EI}}\sin(\gamma - \theta). \tag{4}$$

The relation between θ and γ can be obtained by searching the root of the function for a given γ. To avoid an unstable state when γ reaches 180° (i.e. no out-of-plane torque to maintain the catheter in the azimuthal plane), γ must remain less than 180°. The flexural rigidity can be estimated using the relation introduced in equation (4).

2.2. Forward kinematics of the magnetic continuum device

The majority of continuum devices use insertion/retraction and shaft rotation to control distal tip position. In cardiac surgery the RF catheter is inserted into the heart chamber through a semi-rigid insertion sheath, which allows for the transmission of the insertion and rotation motion along the catheter shaft. Endoscopes for navigation in the gastro-intestinal tract have a 2.8 mm tool channel, and insertion or rotation motion can be transferred to the distal end as for cardiac catheters. Mechanical rotation motion is represented by ϕ_0 and the mechanical translation motion by $\boldsymbol{d}_0$. The resulting transformation for the mechanical motion is:

$$\boldsymbol{T}_0^1 = \begin{pmatrix} \cos(\phi_0) & -\sin(\phi_0) & 0 & 0 \\ -\sin(\phi_0) & \cos(\phi_0) & 0 & 0 \\ 0 & 0 & 1 & \boldsymbol{d}_0 \\ 0 & 0 & 0 & 1 \end{pmatrix} \tag{5}$$

Assuming a constant curvature, a continuum device can be defined by a set of arc parameters. [36] The constant curvature arc is defined by a curvature κ, an in-plane rotation angle ϕ, and a segment length $\boldsymbol{l}$. The coordinate system for the distal end is set at the distal end of the insertion sheath or the tool channel with the z-axis aligned with the continuum device longitudinal axis. The configuration space is parameterized with $\boldsymbol{q} = [\phi_0, \boldsymbol{d}_0, \phi_1, \kappa_1, \boldsymbol{l}_1, \phi_2, \kappa_2, \boldsymbol{l}_2, \phi_3, \kappa_3, \boldsymbol{l}_3]$ for a two segment variable stiffness continuum device, with the index $\boldsymbol{i}$ representing the i[th] segment [37]. The resulting transformation for one variable stiffness segment is:

$$\begin{aligned} \boldsymbol{T}_1^2 &= \boldsymbol{rotz}(\phi_1)\boldsymbol{T}_{\boldsymbol{inPlane}}(\kappa_1, \boldsymbol{l}_1) \\ &= \begin{pmatrix} \cos(\phi_1)\cos(\kappa_1\boldsymbol{l}_1) & -\sin(\phi_1) & \cos(\phi_1)\sin(\kappa_1\boldsymbol{l}_1) & \dfrac{\cos(\phi_1)(1-\cos(\kappa_1\boldsymbol{l}_1))}{\kappa} \\ -\sin(\phi_1)\cos(\kappa_1\boldsymbol{l}_1) & \cos(\phi_1) & \sin(\phi_1)\sin(\kappa_1\boldsymbol{l}_1) & \dfrac{\sin(\phi_1)(1-\cos(\kappa_1\boldsymbol{l}_1))}{\kappa_1} \\ -\sin(\kappa_1\boldsymbol{l}_1) & 0 & \cos(\kappa_1\boldsymbol{l}_1) & \dfrac{\boldsymbol{sin}(\kappa_1\boldsymbol{l}_1)}{\kappa_1} \\ 0 & 0 & 0 & 1 \end{pmatrix}. \end{aligned} \tag{6}$$

When the curvature is zero the transformation is given by:

$$\boldsymbol{T}_1^2 = \boldsymbol{rotz}\left(\phi_1\right)\boldsymbol{T}_{\boldsymbol{inPlane}}\left(\kappa_1, \boldsymbol{l}_1\right) = \begin{pmatrix} \cos\left(\phi_1\right) & -\sin\left(\phi_1\right) & 0 & 0 \\ -\sin\left(\phi_1\right) & \cos\left(\phi_1\right) & 0 & 0 \\ 0 & 0 & 1 & \boldsymbol{l}_1 \\ 0 & 0 & 0 & 1 \end{pmatrix} \quad (7)$$

To combine the motion from multiple variable stiffness segments, the transformation matrices for each segment are multiplied.

3. Results

3.1. Thermal characterization

Thermal characterization of the VS continuum device is performed in air at room temperature (24°C) and in water at body temperature (37°C without forced flow) to mimic a real case scenario. The surface temperatures of the device are measured by two thermistors (SMD 0402, Vishay) glued on the device's external surface at the center of one of the heaters (measuring temperature T1) and 10 mm away from the heater center (measuring temperature T2). The device is heated for the first 60 s of the experiment. For the rest of the experiment, no current is applied and the heater naturally cools in the environment. The heater has a resistance R_0 of 2.15 Ω at T0 = 24°C with the wires extending 100 mm outside of the heater. The wires are connected to a larger cross section wire to limit the self-heating of long connecting wires. The maximum current in the heater is limited to 1 A to avoid damage to the heating wire. The resulting variations of the resistance of the heater are shown in **Figure 3A** and corresponding temperature measures in **Figure 3B.**

In both air and water, the melting and the solidification of the LMPA are indicated by the two plateaus clearly visible on the heater resistance measurement during the heating phase (at R=2.30 Ω) and the cooling phase (at R=2.27 Ω). This shows that stiffness control can be robustly performed using the resistance measurement. Thresholds for the hysteresis controller

can thus be selected based on this experiment, after identification of the plateau corresponding to the phase change of the LMPA. One can see that the thermistors' temperatures on the corresponding plateau are different in air and in water. This can be explained by the fact that the thermistors are mounted on the outer surface of the silicone tube and are not directly in contact with the heater. The maximum temperature reached after the heating process in air and water are 60°C and 41°C, respectively, on the outer surface of the device.

The melting time (i.e. the time needed to completely melt the VSS during the heating phase) is approximately 15 s in both cases. Starting from a temperature of 41°C, which constitutes the higher thermal limit to avoid damage to the body, the cooling time needed for the complete solidification of the VSS is faster in water (20 s) than in air (80 s), consistent with the relative high heat transfer capability of water with respect to air.

The stiffness transition (solid to liquid) can be obtained in water with external temperatures T1 and T2 less than 41°C, thus ensuring no thermal damage to human cells.

3.2. Stiffness control demonstration

To test stiffness control, a VS continuum device is placed inside a rotating magnetic field and is maintained in the soft state with a hysteresis controller. The magnetic field oscillates between -90° and 90° with an angular speed of 30°/s; at 90° and -90° the magnetic field is maintained constant for one second. The rotating magnetic field is used to measure the deflection amplitude over time. The heating starts at t=0s when the active hysteresis controller turns on the heating, and **Figure 4A** shows the heater resistance and deflection amplitude over time. During the first twenty seconds we observe the plateau corresponding to the LMPA phase change between solid and liquid, and after turning off the heater the plateau corresponding to the LMPA phase change from liquid to solid.

In **Figure 4B**, the correlation between deflection amplitude and heater resistance is represented. The deflection amplitude is measured between two deflection peaks and is an

average between two discrete measurements separated by seven seconds. The point t1 on the plot represents the resistance at t =12 s and the deflection amplitude between measurements at 5 s and 12 s. The initial heating is too fast to provide a reliable measurement of deflection amplitude variation as the deflection was close to zero at 5 s and close to the steady state at 12 s. Once the LMPA is melted the hysteresis controller maintains the resistance between the thresholds to avoid overheating or LMPA solidification. This results in maintaining the deflection amplitude close to a constant value of 30°. When the continuum device cools and solidifies, we observe a drop of the deflection amplitude with only a limited change of heater resistance (i.e. LMPA solidification temperature plateau). Once the LMPA has solidified the continuum device is rigid and the temperature continues to decrease.

3.3. Deflection in soft and stiff states

Two key device characteristics that must be determined are softness and stiffness. Softness is determined by deflection in a specific magnetic field when one of its segments is in the liquid state. Stiffness is determined by investigating the effect of the magnetic torque when the segments are in their solid state, which governs the level of shape fixity that can be achieved. The deflection for our VS continuum devices prototype is characterized inside the CardioMag (the Aeon Phocus non-clinical prototype) with a magnetic field magnitude of 80mT and varying magnetic field orientations. The VS continuum device tested has three segments. A hysteresis controller was used to maintain a VSS in the soft state.

In the rigid state, the VSS is not significantly deflected at the maximum magnetic torque of 2 x 10^{-3}Nm, obtained by applying a magnetic field magnitude of 80 mT and a misalignment angle of 90° (**Figure 5A**). The configuration of the overall catheter does not influence its shape fixity capability within this range of torques and tip curvatures.

In the soft state, the magnetic field inclination was varied between 0° and 150° in both directions. As represented in **Figure 5B-D**, it is possible to deflect each of the VSS segments

independently more than 100°. The deflection of VSS3 was larger as it carries the weight of the two distal segments and the tip magnet. Using equation (4) and an estimation of each parameter, we obtain an estimate for the flexural rigidity of 5 x 10^{-6}Nm^2.

To increase the deflection of a single VSS, the magnetic volume or the magnetic field can be increased. Depending on the desired operating volume, the variable stiffness segment length can also be increased. In this case, a length increase has the advantage of not being affected by a possible non-linearity of the elasticity module for large deflection angles.

The current injected into the VSS generates a magnetic torque that is negligible, being approximately two orders of magnitude smaller than the one generated by the permanent magnet. No impact of the additional dipole moment due to the heaters has been observed when turning on and off the heater in a static magnetic field while one of the segments is in a soft state.

3.4. Constant stiffness workspace

A constant stiffness workspace is a workspace that can be explored without a change of stiffness, meaning there are no heating or cooling delays (**Figure 6A**, Movie S4). During an MIS procedure, it would be of particular interest to operate in one of these constant stiffness workspaces.

From the measured deflection characteristics of our variable stiffness continuum devices, we can simulate the reachable workspace assuming constant curvature using the forward kinematics (Section 2.3.3.). To select a constant stiffness workspace and the corresponding continuum device shape, we can explore all continuum device shapes for reaching target positions. A simplification for exploring all possible shapes can be obtained by observing that the parameters ϕ_0 and ϕ_1 define a rotation around the same axis. Removing the mechanical rotation does not reduce the possible continuum device shapes and final position but does reduce the number of trajectories to reach these end effector positions. To determine all

possible configurations to reach a target position in task space we can compute all possible continuum device shapes for varying parameters, excluding ϕ_0, ϕ_1 and d_0. The set of configurations that have the same radial distance from the insertion axis can reach the position in task space by mechanical insertion d_0 and mechanical rotation ϕ_0. In **Figure 6B** the planar continuum device configurations that reach a target position are represented. It can be observed that a variety of continuum device shapes with different tip orientations can reach a single target position. This can be extended to non-planar shapes to further increase the diversity of configurations and tip orientations.

Each of the continuum device configurations results in a different constant stiffness workspace. A well-selected constant stiffness workspace reduces the number of stiffness changes required during a particular procedure, thus reducing the time it takes to perform a given task.

3.5. Mechanical actuation and magnetic actuation

In a given stiffness state, the degrees of freedom available are the mechanical rotation, mechanical insertion/retraction, and tip deflection with the magnetic field. With the VS continuum device inserted inside an introducer sheath, the mechanical insertion/retraction moves the continuum device tip in a motion collinear to the insertion axis (**Figure *7*A**) and the mechanical rotation in a circular trajectory centered on the insertion axis (**Figure *7*B**). Creating a contact between an MIS instrument and organ tissue requires the ability to move the tip of an instrument forward. This motion is primarily performed by mechanical insertion and rotation. Tip deflection changes the instrument orientation but not its length. In a constant stiffness state, simultaneous control of the tip position and orientation (i.e. 6 DOF) is not possible, because there are only four control variables, but for purely position control, we have one redundant control parameter. This means that hysteresis and error in the rigid segments shape can be corrected with mechanical actuation and magnetic actuation.

The position precision depends on the precision of the position feedback system and the closed-loop control algorithms. The mechanical actuation and the magnetic actuation allow precise and fast motion with delay less than 200ms allowing an algorithm to close the loop and achieve submillimeter position precision.[38] Hysteresis and error in the mechanical actuation and magnetic actuation can be directly compensated by closed-loop control.

In a scenario close to a cardiac arrhythmia ablation, we demonstrated that the user can control the magnetic field direction at the center of the workspace and the catheter insertion length to reach a target tip position.[9] The uniformity of the magnetic field in the workspace is sufficient, and inhomogeneity of the magnetic field did not disturb the user. Similar results are expected with our VS continuum device, since in a given stiffness state the dynamics are similar to a conventional magnetic catheter, and fine position control only relies on mechanical actuation and mechanical actuation.

The VS has been shaped repeatedly with the magnetic field for more than 5 hours without observable fatigue (**Movie S6** show 600s of operation). In our previous prototype without an inner lumen,[24] fatigue was observed due to rigid deformation of the copper wire. The inner lumen not only provides a working channel, but also maintains the heating wire in its original position.

4. Discussion and Conclusion

The VS magnetic continuum device provides a significant increase in manipulability compared to available magnetic continuum devices. Its small diameter and central working channel allow for its use in several minimally invasive procedures in organs with small diameter access paths, such heart chambers and the gastrointestinal tract. If used in the context of cardiac arrhythmia ablation, the VS magnetic continuum device enables multiple bending radii and reduces the number of magnets from 3 to 1 as compared to traditional

magnetic catheters. It can selectively soften for deflection under the magnetic field comparable to flexible catheters, or rigidify for better stability. Due to the multiple VS sections and integrated temperature control, the deformation can be locally controlled in tens of seconds, enabling for example a part of the VS catheter to maintain an optimal compliance for a larger range of insertion lengths. For gastrointestinal endoscopy, VS magnetic continuum devices can be directly inserted into the tool channel (internal diameter ranging between 2.8mm and 3.8mm depending on the particular endoscope [39]) of existing endoscopes to provide precise tool control and multiple bending locations without increasing the overall endoscope diameter. [40]

With the increased dexterity comes new challenges that will require the development and integration of 3D shape detection algorithms, path planning algorithms, closed-loop control algorithms, a mechanical advancer unit, and an intuitive control interface for the surgeon. Additionally, fundamental work on thermal modeling, thermal control, characterization methods, and improvement of the manufacturing process is needed.

Supporting Information

Supporting Information is available from the Wiley Online Library or from the author.

Acknowledgements

This work has been partially supported by the Swiss National Science Foundation through grant number 200021_165564, the National Center of Competence in Research (NCCR) Robotics, and the ERC Advanced Grant 743217 Soft Micro Robotics (SOMBOT)

Received: ((will be filled in by the editorial staff))
Revised: ((will be filled in by the editorial staff))
Published online: ((will be filled in by the editorial staff))

References

1. J. Burgner-Kahrs, D.C. Rucker, H. Choset, *IEEE Trans. Robot*, **2015**, *31 (6)*, 1261–1280.

2. Z. Li, L. Wu, H. Ren, H. Yu, *Mech. Mach. Theory* **2017**, *107*, 148–165.

3. N. Simaan, K. Xu, W. Wei, A. Kapoor, P. Kazanzides, R. Taylor, P. Flint, *Int. J. Rob. Res.* **2009**, *28 (9)*, 1134–1153.

4. P. Sears, P. Dupont, *IEEE Int. Conf. Intell. Robot. Syst.* **2006**, *2850-2856*

5. M. Cianchetti, T. Ranzani, G. Gerboni, I. De Falco, C. Laschi, A. Menciassi, *IEEE Int. Conf. Intell. Robot. Syst.* **2013**, 3576–3581.

6. J. Jayender, M. Azizian, R.V. Patel, *IEEE Trans. Robot.* **2008**, *24 (4)*, 858–871.

7. J.H. Crews, G.D. Buckner, *J. Intell. Mater. Syst. Struct.* **2012**, *23 (5)*, 545–562.

8. C. Pappone, G. Vicedomini, F. Manguso, F. Gugliotta, P. Mazzone, S. Gulletta, N. Sora, S. Sala, A. Marzi, G. Augello, L. Livolsi, A. Santagostino, A., V. Santinelli, *J. Am. Coll. Cardiol.* **2006**, *47 (7)*, 1390–1400.

9. C. Chautems, S. Lyttle, Q. Boehler, B.J. Nelson, *IEEE Robot. Autom. Lett.* **2018**, *3 (3)*, 2123–2128.

10. C. Chautems, B.J. Nelson, *IEEE Int. Conf. Robot. Autom.* **2017**, 4837–4842.

11. M.S. Grady, M.A. Howard, R.G. Dacey, W. Blume, M. Lawson, P. Werp, R.C. Ritter, *J. Neurosurg.* **2000**, *93 (2)*, 282–288.

12. J. Edelmann, A.J. Petruska, B.J. Nelson, *J. Med. Robot. Res.* **2017**, *3*, 1850002.

13. J.R. Clark, L. Leon, F.M. Warren, J.J. Abbott, *2011 IEEE/RSJ Int. Conf. Intell. Robot. Syst.* **2011**, 1321–1326.

14. S.L. Charreyron, B. Zeydan, B.J. Nelson, *IEEE Int. Conf. Robot. Autom.* **2017**, 4843–4848.

15. K.R.J. Chun, B. Schmidt, B. Köktürk, R. Tilz, A. Fürnkranz, M. Konstantinidou, E. Wissner, A. Metzner, F. Ouyang, K.-H. Kuck, *Herz* **2008**, *33 (8)*, 586–589.

16. A. Loeve, P. Breedveld, J. Dankelman, *IEEE Pulse* **2010**, *1 (3)*, 26–41.

17. Y. Chen, J.H. Chang, A.S. Greenlee, K.C. Cheung, A.H. Slocum, R. Gupta, *IEEE Int. Conf. Robot. Autom.* **2010**, 5570–5575.

18. K. Ikuta, H. Ichikawa, K. Suzuki, D. Yajima, *IEEE Int. Conf. Robot. Autom.* **2006**,

4161–4166.

19. R. Zhao, Y. Yao, Y. Luo, *J. Med. Device.* **2016**, *10 (2)*, 021002.
20. M. Cianchetti, T. Ranzani, G. Gerboni, T. Nanayakkara, K. Althoefer, P. Dasgupta, A. Menciassi, *Soft Robot.* **2014**, *1 (2)*, 122–131.
21. Y.-J. Kim, S. Cheng, S. Kim, K. Iagnemma, *IEEE/RSJ Int. Conf. Intell. Robot. Syst.* **2012**, 4251–4256.
22. S. Griffin, US 7828790 B2, **2004**.
23. H. Dong, G.M. Walker, *Smart Mater. Struct.* **2012**, *21 (4)*, 042001.
24. C. Chautems, A. Tonazzini, D. Floreano, B.J. Nelson, *IEEE/RSJ Int. Conf. Intell. Robot. Syst.* **2017**, 181–186.
25. G. Stabile, F. Solimene, L. Calò, M. Anselmino, A. Castro, C. Pratola, P. Golia, N. Bottoni, G. Grandinetti, A. De Simone, R. De Ponti, S. Dottori, E. Bertaglia, *Europace* **2014**, *16 (3)*, 335–40.
26. J.K.-R. Chun, S. Ernst, S. Matthews, B. Schmidt, D. Bansch, S. Boczor, A. Ujeyl, M. Antz, F. Ouyang, K.-H. Kuck, *Eur. Heart J.* **2007**, *28 (2)*, 190–195.
27. I.M. Van Meerbeek, B. C. Mac Murray, J.W. Kim, S.S. Robinson, P.X. Zou, M.N. Silberstein, R.F. Shepherd, *Adv. Mater.* **2016**, *28 (14)*, 2801–2806.
28. B.E. Schubert, D. Floreano, *RSC Adv.* **2013**, *3 (46)*, 24671.
29. L. Yi, J. Liu, *Int. Mater. Rev.* **2017**, 1–26.
30. A. Tonazzini, S. Mintchev, B. Schubert, B. Mazzolai, J. Shintake, D. Floreano, *Adv. Mater.* **2016**, *28 (46)*, 10142–10148.
31. C. Liu, H. Qin, P.T. Mather, *J. Mater. Chem.* **2007**, 17 (16), 1543.
32. S. Ernst, F. Ouyang, C. Linder, K. Hertting, F. Stahl, J. Chun, H. Hachiya, D. Bänsch, M. Antz, K.-H. Kuck, *Circulation* **2004**, *109 (12)*, 1472–5.
33. J.J. Abbott, O. Ergeneman, M.P. Kummer, A.M. Hirt, B.J. Nelson, *IEEE Trans. Robot.* **2007**, 23 (6), 1247–1252.

34. I. Tunay, *26th Annu. Int. Conf. IEEE Eng. Med. Biol. Soc.* **2004**, *3*, 2006–2009.

35. I. Tunay, *Proc. IEEE Int. Conf. Mechatronics* **2004**, 392–397.

36. R.J. Webster, B.A. Jones, *Int. J. Rob. Res.* **2010**, *29 (13)*, 1661–1683.

37. M.W. Hannan, I.D. Walker, *J. Robot. Syst.* **2003**, *20 (2)*, 45–63.

38. J. Edelmann, A.J. Petruska, B.J. Nelson, *Int. J. Rob. Res.* **2017**, 36 (1), 68–85.

39. J.T. Maple, B.K. Abu Dayyeh, S.S. Chauhan, J.H Hwang, S. Komanduri, M. Manfredi, V. Konda, F.M. Murad, U.D. Siddiqui, S. Banerjee, *Gastrointest. Endosc.* **2015**, *81 (6)*, 1311–1325.

40. H.C. Koo, J.H. Moon, H.J. Choi, B.M. Ko, S.J. Hong, Y.K. Cheon, Y.D. Cho, J.S. Lee, M.S. Lee, C.S. Shim, *Gastrointest. Endosc.* **2009**, *69 (4)*, 931–934.

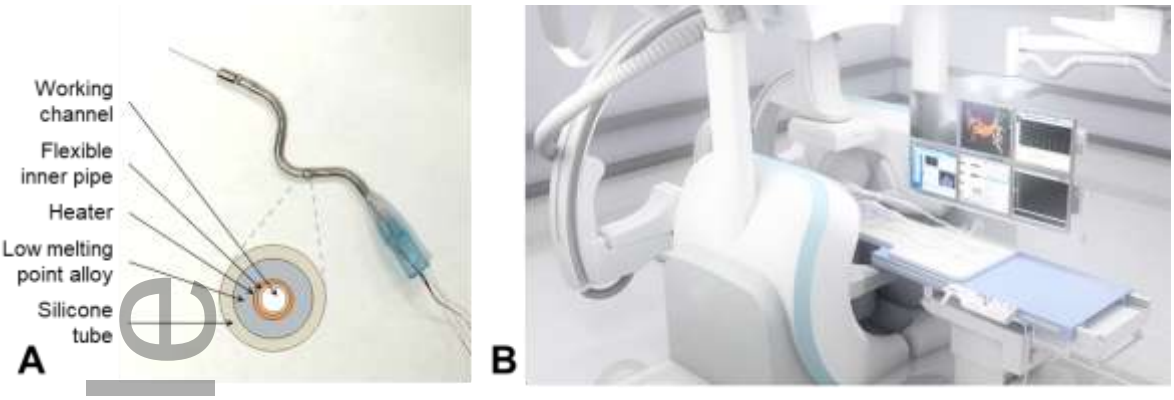

Figure 1. (**A**) VS magnetic continuum device with a central working channel. (**B**) Magnetic manipulation system Aeon Phocus integrated with Artis Zee angiography system.

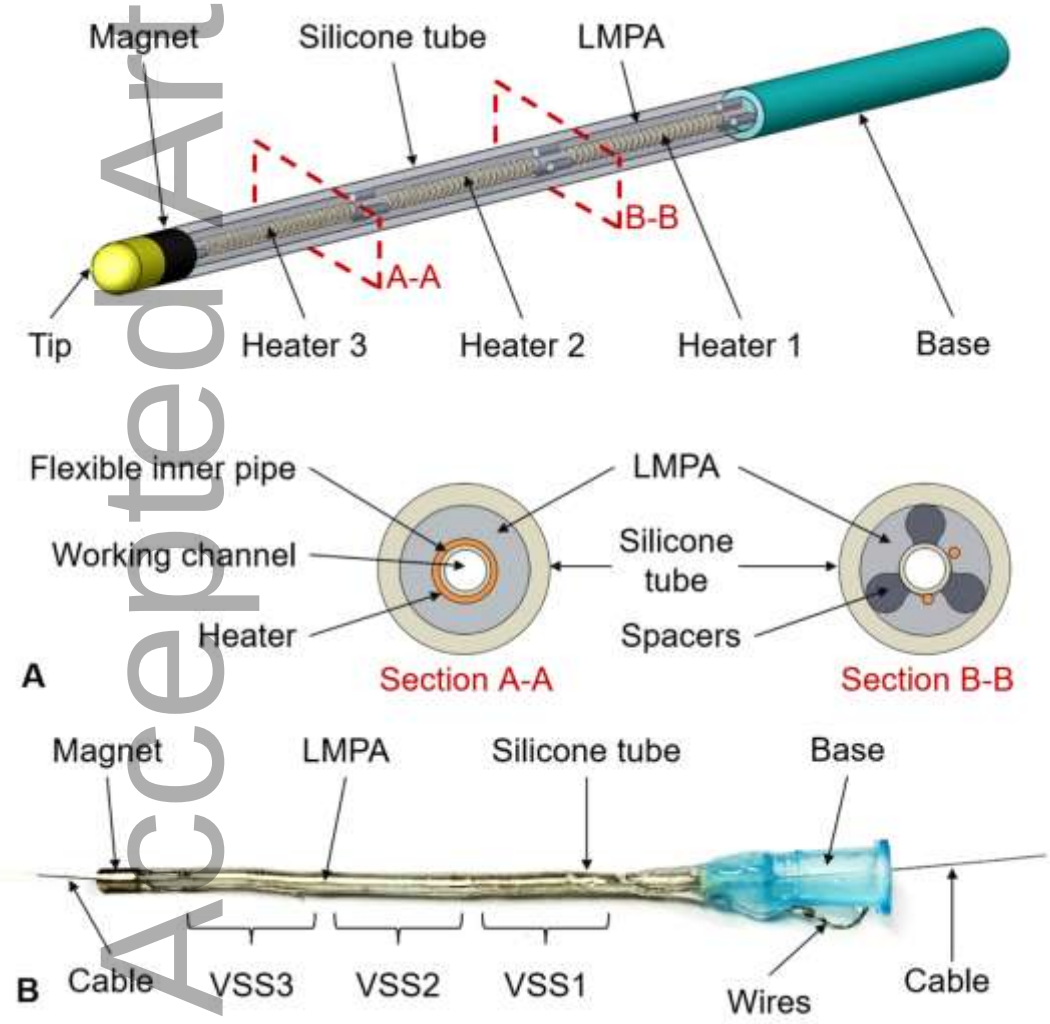

Figure 2. Magnetic continuum device based on LMPA characterized by a central working channel and three VS segments. **(A)** Schematic of the prototype with two different sections highlighted to show the components. **(B)** Pictures of the working prototype. A cable that passes through the device highlights the presence of the central working channel.

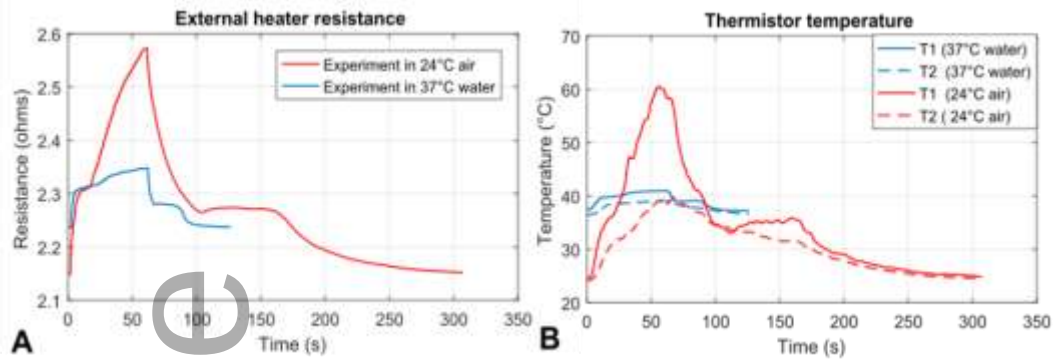

Figure 3. Results of thermal characterization in air at 24°C (red) and in water at 37°C (blue). (**A**) Representative curves of the heater resistance over time in the two cases. (**B**) Representative curves of the surface temperature measured with thermistors corresponding to the heater (T1) and 10 mm from the heater (T2).

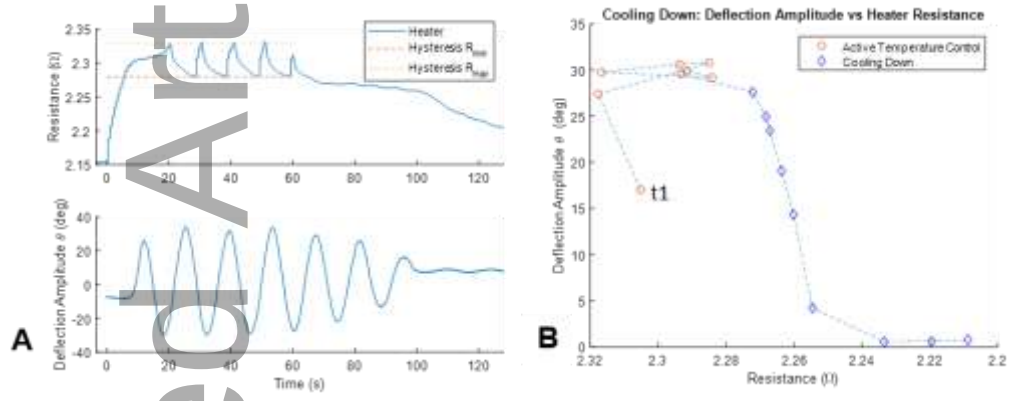

Figure 4. Results of stiffness control for a variable stiffness catheter with $\boldsymbol{R}_{\min} = 2.28\,\Omega$ and $\boldsymbol{R}_{\max} = 2.32\,\Omega$. (**A**) Measurement of heater resistance and deflection amplitude in a rotating magnetic field between -90° and 90° in air. (**B**) Correlation between resistance and tip deflection amplitude.

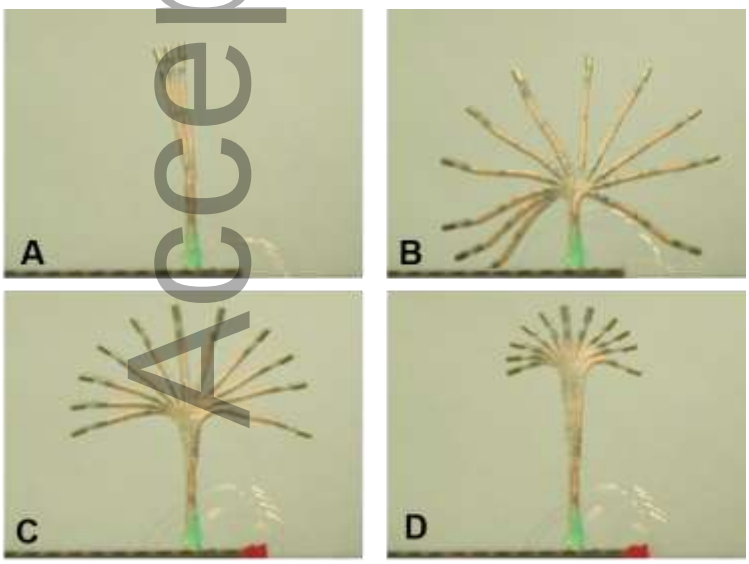

Figure 5. Cumulative image representing the deflection of our VS magnetic continuum devices. **(A)** The three VS segments are in rigid states and magnetic field inclination is changed between -90° and 90° **(B)** VSS1 in the soft state and magnetic field inclination is changed between 150° and 150°. **(C)** VSS2 in the soft state and magnetic field inclination is

changed between -150° and 150°. (**D**) VSS3 in soft state and magnetic field inclination is changed between -150° and 150°.

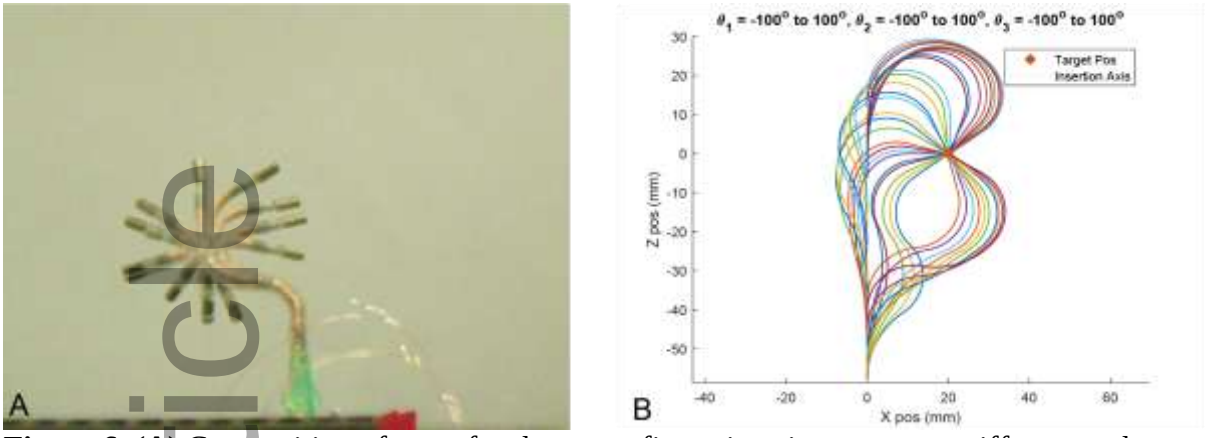

Figure 6. (A) Composition of sets of catheter configurations in a constant stiffness workspace (VSS1-2: rigid, VSS3: soft) (**B**) Set of planar configurations to reach a target tip position.

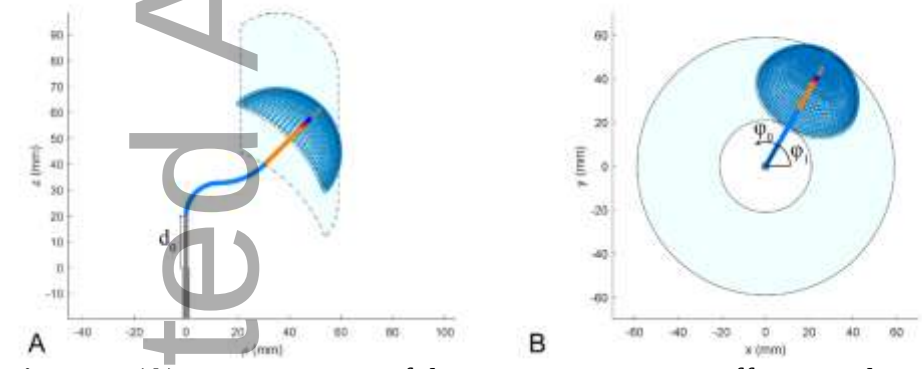

Figure 7. (**A**) Representation of the insertion constant stiffness workspace in cyan with the set of continuum device distal positions (blue circle) for a given insertion length. (**B**) Representation of the rotation workspace in cyan with the set of continuum device tip distal positions (blue circle) for a given rotation angle.

Keyword: soft robotics

A Magnetic Continuum Device with Variable Stiffness for Minimally Invasive Surgery

Christophe Chautems[*]*, Alice Tonazzini, Quentin Boehler, Seung Hee Jeong, Dario Floreano, Bradley J. Nelson*

A variable stiffness continuum device controlled by external magnetic fields for medical applications. The device is composed of several sections which stiffness is controlled to be either stiff or soft. The magnetic torque is used to remotely control the shape of the soft sections while the stiff sections remain unchanged, thus adding degrees of freedom to the magnetic continuum device.